Available online at www.sciencedirect.com
ScienceDirect
Catalysis Today 119 (2007) 219–227
CATALYSIS TODAY
www.elsevier.com/locate/cattod

Computational spectroscopy and DFT investigations into nitrogen and oxygen bond breaking and bond making processes in model *de*NO_x and *de*N_2O reactions

Piotr Pietrzyk [a], Filip Zasada [a], Witold Piskorz [a], Andrzej Kotarba [a], Zbigniew Sojka [a,b,*]

[a] *Faculty of Chemistry, Jagiellonian University, Ingardena 3, 30-060 Kraków, Poland*
[b] *Regional Laboratory for Physicochemical Analyses and Structural Research, Jagiellonian University, Ingardena 3, 30-060 Kraków, Poland*

Available online 18 September 2006

Abstract

Molecular DFT modeling combined with computational spectroscopy (EPR and IR) were applied for analysis of the N–O bond breaking and N–N and O–O bond making in the context of *de*NO_x and *de*N_2O reactions. Interaction of NO, N_2O and NO_2 with cationic (transition metals) and anionic (surface O^{2-} ions) centers was explored at the molecular level. The elementary events such as reactant coordination, charge and spin redistributions, which are principal molecular constraints for efficient decomposition of the nitrogen oxides (N_2O and NO) were discussed. Particular attention was paid to dynamics of the N–O bond cleavage in N_2O molecule through electron and oxygen atom transfer routes, evaluation of preferable coordination modes of NO, discrimination between inner- and outer-sphere mechanism of N–N bond formation, and the influence of spin and electronic redistribution on the reaction course (spin catalysis). Owing to their simplicity and well known surface chemistry, model systems selected for studies of such processes include MoO_x/SiO_2, MgO and ZSM-5 zeolite exchanged with various transition metal ions (TMI) of different electron configuration and spin multiplicity: Mo^{5+} (d^1, ^2D) Fe^{3+}, Mn^{2+}, Cr^+ (d^5, ^6S), Fe^{2+} (d^6, ^5D), Co^{2+} (d^7, ^4F), Ni^{2+} (d^8, ^3F), Cu^{2+} (d^9, ^2D) and Cu^+, Zn^{2+} (d^{10}, ^1S).
© 2006 Elsevier B.V. All rights reserved.

Keywords: NO; N_2O; EPR; DFT; IR; Modeling; ZSM-5; Electron transfer; Spin catalysis; MgO; Transition metals; *de*NO_x; *de*N_2O; Spectroscopy; Mechanism

1. Introduction

Direct decomposition of nitrogen oxides (NO and N_2O) to N_2 and O_2 is a topic of great interest for environmental atmospheric chemistry [1–5]. Despite of their thermodynamic instability (a sacrificial reductant is then not necessarily required), they are kinetically inert with respect to decomposition into N_2 and O_2 molecules. Thus, this reaction requires a catalyst to be efficient for practical applications. However, in spite of the progress made, none of the many catalysts developed until now exhibit satisfactory performance, especially in the presence of water and oxygen excess [2,6].

Transition metal ions (TMI) exchanged into zeolites, supported on oxide carriers, bulk oxides are among typical catalytic materials of *de*NO_x and *de*N_2O catalysis, widely applied in many model and practically-oriented investigations [1,2,7–9]. In this context molecular level knowledge on interaction of NO, N_2O and NO_2 with cationic (transition metals) and anionic (surface O^{2-} ions) centers is of fundamental importance for elucidation of the mechanism, and understanding the elementary surface events such as reactant coordination, charge and spin redistributions, N–O bond breaking and N–N, O–O bond formation processes. A noteworthy feature of those reactions is a spectacular spin redistribution on passing from nitric or nitrous oxide to dinitrogen and dioxygen. The resultant spin barrier along with orbital symmetry violation creates principal molecular constraints for efficient decomposition of the both nitrogen oxides in conceivably simplest concerted way [10,8].

* Corresponding author at: Faculty of Chemistry, Jagiellonian University, Ingardena 3, 30-060 Kraków, Poland. Tel.: +48 12 663 22 95; fax: +48 12 634 05 15.
E-mail address: sojka@chemia.uj.edu.pl (Z. Sojka).

0920-5861/$ – see front matter © 2006 Elsevier B.V. All rights reserved.
doi:10.1016/j.cattod.2006.08.054

Two principal mechanisms along which the nitrous oxide can be decomposed involve dissociative electron transfer (ET) [11] and oxygen atom transfer [12]. In the former case, the electron is supplied by transition metal ions acting as surface electron donor centers (for reductive activation of the N_2O reactant), and electron acceptor centers (for recombination of the resultant O^- intermediates), constituting the cationic redox mechanism. An alternative oxygen atom transfer route may also occur with the participation of transition metal ions, particularly iron [2,8], giving rise to metal-oxo group (FeO^+) and its associated C–H bond hydroxylation chemistry [13,14]. A different pathway involves surface O^{2-} centers with the formation of surface peroxide intermediates O_2^{2-} (anionic redox mechanism). Subsequent recombination of the peroxide species restores the initial surface O^{2-} sites with concomitant production of dioxygen [12,15].

The aim of this contribution is to provide an insight through DFT modeling corroborated with spectroscopic EPR and IR investigations into binding and activation of nitrogen oxides (N_2O and NO) on various surface transition metal ions of different electron configuration (d^1–d^{10}) and spin multiplicity. Particular attention was paid to dynamics of the N–O bond cleavage in N_2O molecule through electron and oxygen atom transfer route, evaluation of preferable coordination modes of NO, discrimination between the inner- and outer-sphere mechanism of N–N bond formation and the influence of spin and electronic redistribution on the reaction course (spin catalysis). Owing to their simplicity and well known surface chemistry suitable model functional systems selected for the study of such processes are MoO_x/SiO_2, TMI/ZSM-5 and MgO.

2. Molecular modeling and computational spectroscopy

DFT modeling of complex heterogeneous catalytic systems constituted by transition metals of various spin multiplicity appears to be computationally quite demanding. Judicious selection of an appropriate cluster model and adequate calculation scheme (electron-correlation functional, basis sets, etc.) are of great importance for obtaining sensible results. In our method of exploring the mechanism of catalytic reactions we combine molecular modeling with computational spectroscopy. Spectroscopic parameters of the postulated active sites, reaction intermediates, transients, spectators and final products are calculated to be directly compared with available experimental data (magnetic EPR parameters and IR frequencies and intensities). Such approach provides not only a quantitative bridge between the molecular structure of investigated species and their spectroscopic fingerprints, but it can also be used for guiding molecular modeling of the investigated catalytic reactions, providing useful check points justifying the adequacy of both the adopted model and the method as well.

Periodic calculations were carried out with CASTEP code [16,17] using PW91 correlation-exchange potential. The unit cell optimization was based on BFGS Hessian update scheme [18]. The calculated Hirshfeld [19,20] atomic charges (±0.605 for Mg and O ions) were next used for electrostatical embedding of MgO cluster in the lattice of the corresponding point charges (PC-s).

The cluster computations were carried out with DMol^3 [21] software with implemented Delley's scheme [22]. The local density approximation (LDA) in VWN parameterization [23] and the DNP basis set with frozen inner core and the integration grid of fine density were used. The geometry optimization was performed for all the ions but those linked directly to at least one PC. The Mayer valence analysis was used while calculating bond orders [24].

For cluster modeling a flat surface was cut off from the (1 0 0) plane of MgO to form a hemisphere of the radius of 6.3 Å, extended next to 20.0 Å by an array of PC-s reproducing the lattice Madelung potential. The stoechiometry of the resultant cluster was $Mg_{40}O_{40}(PC_{1836})$. The (1 0 0) surface was chosen because it has been recently found that penta-coordinated oxygen ions located on this face are actually responsible for N_2O decomposition on MgO in the steady state conditions [25].

The interaction of NO with TMI dispersed within ZSM-5 zeolite lattice was modeled at the VWN/DNP level. In order to obtain more accurate energy values, a posteriori correction $\Delta E_{\text{total}} = E_{\text{XC}}^{\text{GGA}} \lfloor \rho^{\text{LSDA}} \rfloor - E_{\text{XC}}^{\text{LSDA}} \lfloor \rho^{\text{LSDA}} \rfloor$ based on the perturbative GGA with the BPW91 [26,27] exchange-correlation functional was applied. The zeolite centers hosting the cations were modeled with **M5** $[Si_4AlO_5(OH)_{10}]^-$ and **Z6** $[Si_4Al_2O_6(OH)_{12}]^{2-}$ clusters, cut off from the MFI structure. The boundary atoms were replaced by hydrogen atoms and geometry of the clusters was optimized with their positions constrained at the points defined by the framework. The molybdenum surface complexes $\{Mo_{4c}^{5+}\}/SiO_2$ and $\{O^- - Mo_{4c}^{5+}\}/SiO_2$ were modeled with {Mo=O(OH)}/**T2** and {O–Mo=O(OH)}/**T2** clusters, respectively.

The vibrational analysis was performed using the double harmonic approximation. The Hessian matrices were evaluated by numerical differentiation (one-point finite difference) of the analytic energy gradients using a displacement of 0.01 bohr from the optimized geometry for all 3*N* coordinates. No scaling factors were used. All single-point calculations of ***g*** tensor were performed with the ADF [28–30] version 2004.01 program. As a standard the triple-ζ valence Slater-type orbital basis set plus a set of polarization functions (TZP) was used for all atoms with the gauge dependence solved by using GIAOs. To account for relativistic effects spin-orbit coupling was included variationally within ZORA method [31]. The spin-unrestricted calculations were carried out within the collinear approximation [32]. As for the ***A*** tensor we used Gaussian03 with BPW91 exchange-correlation functional with a combination of LanL2DZ and 6-311G(d) basis sets [33].

The EPR and IR spectra were recorded using BRUKER X-band ELEXYS-500 and ISF 48 spectrometers, respectively. Simulations of EPR spectra joint with hybrid genetic algorithm optimization were performed by means of EPRsim32 program [34]. Temperature programmed surface reaction (TPSR) studies of N_2O decomposition over model catalysts were carried out using a tubular quartz reactor and QMS (RGA200, Stanford Research System) monitoring of the reaction products.

Preparation of grafted 0.33 wt.% MoO_x/SiO_2 sample was described elsewhere [35]. TMI/ZSM-5 samples were obtained from parent NH_4/ZSM-5 zeolite (Zeolyst, Inc.) by standard ion

exchange procedure from the corresponding nitrate solutions [36], whereas 1 wt.% Gd/MgO samples were prepared by dry impregnation of MgO (Merck) with aqueous solution of gadolinium nitrite (Aldrich).

3. Results and discussion

3.1. Mechanistic pathways for decomposition of N_2O

3.1.1. Electron transfer route

Catalytic decomposition of N_2O based on electron transfer follows a classic three-step mechanism

$$N_2O(^1\Sigma^+) + e^- \rightarrow O^-(^2P) + N_2{}^{\uparrow}(^1\Sigma_g{}^+)$$

$$O^-(^2P) + O^-(^2P) \rightarrow 2e^- + O_2{}^{\uparrow}(^3\Sigma_g{}^-)$$

$$O^-(^2P) + N_2O(^1\Sigma^+) \rightarrow e^- + O_2{}^{\uparrow}(^3\Sigma_g{}^-) + N_2{}^{\uparrow}(^1\Sigma_g{}^+)$$

involving a transient N_2O^- intermediate and an important spin rearrangement, which constitutes vibronic and spin barriers for this process. To initiate the reaction surface TMIs act as redox centers (allowing for interfacial electron shuttling), molecular templates (providing orbitals of proper energy and symmetry for N_2O binding and ET), and as spin catalysts (facilitating conversion of the spin states). Tetra-coordinated $\{Mo^{5+}_{4c}\}/SiO_2$ surface molybdenyl complexes with $g_{\|} = 1.76$, $g_{\perp} = 1.926$ produced upon reduction of MoO_x/SiO_2 sample were found to function as suitable active sites for this reaction, which using paramagnetic naturally abundant Mo and enriched ^{95}Mo ($I = 5/2$) as a self-probes can easily be followed by EPR spectroscopy [11]. The surface molybdenum ion exhibits a bidentate coordination to the silica framework with nearly equal Mo–O(Si) bond lengths ($<d_{Mo-O(Si)}>1.954(3)$ Å), and the terminal Mo=O bond being much shorter ($d_{Mo=O} = 1.718$ Å). The O(Si)–Mo–O(Si) angle was equal to 98°, whereas O=Mo–O(H) angle was slightly larger (117°), giving rise to a pseudo-tetrahedral structure. The ZORA/VWN calculations were able to reproduce the components of ***g*** tensor using the {Mo=O(OH)}/**T2** cluster quite satisfactorily, yielding $g_{\perp} = {}^1/_2(g_1 + g_2) = 1.916$ and $g_{\|} = 1.745$, confirming thereby the molecular identity of these sites inferred form the spectroscopic studies [11,35]. The $\{Mo^{5+}_{4c}\}/SiO_2$ centers readily binds N_2O at ambient conditions forming a penta-coordinated $\{N_2O - Mo^{5+}_{4c}\}/SiO_2$ complex of C_{4v} symmetry and a SOMO being predominantly d_{xy} ($g_{\|} = 1.87$, $g_{\perp} = 1.957$). Activation of the sample at 373 K leads to thermally induced dissociative ET, producing bound O^- species ($g_{\|} = 2.005$, $g_{\perp} = 2.02$) and free N_2 molecule. A well resolved ^{95}Mo superhyperfine structure ($A_{\|} = 0.78$ mT, $A_{\perp} = 0.67$ mT) provides a clear evidence that the O^- is associated with the Mo center [37]. The calculated ***g*** tensor with $g_{\perp} = {}^1/_2(g_1 + g_2) = 2.018 > g_{\|} = 2.002$ obtained for the square pyramid {O–Mo=O(OH)}/**T2** structure, remains in a good agreement with the experimental values.

A molecular pathway for the dissociative electron transfer process consists in the flow of the electron from the d_{xy} donor orbital toward $3\pi^*$ acceptor orbital of the N_2O ligand with formation of a transient N_2O^- species. The activation energy for ET is found to be 20 ± 4 kJ mol^{-1} from the variable temperature studies in the 323–393 K range [11].

In order to rationalize the results and identify the molecular barriers contributing to the observed activation energy the data inferred from EPR were embedded into the framework of the electron transfer theory [38]. Because the neutral N_2O is linear ($C_{\infty v}$ symmetry), while the corresponding N_2O^- transient is bent (C_s symmetry), there is a Franck-Condon (FC) restriction for the electron transfer (instantaneous geometries of both species must be the same), as the bending of N_2O ligand has to precede the actual ET event. Upon the $C_{\infty v} \rightarrow C_s$ deformation the unpaired electron occupies a 10a′ orbital (derived from $3\pi^*$), which is strongly stabilized as shown in the Walsh diagram (Fig. 1). In the linear form the acceptor orbital ($3\pi^*$, $E_{3\pi} = -2.14$) is situated distinctly above the SOMO of the electron donor center constituted by the surface molybdenum ($E_{3d} = -5.04$ eV), whereas in the angularly distorted geometry (which is assumed as a result of vibronic excitation) the energy of the 10a′ orbital is lowered below the SOMO. Remarkable shift in the energy of this electron accepting orbital (from −2.14 to −6.53 eV upon the bending) opens the pathways for making the ET energetically favorable.

To provide a more in-depth insight into dynamics of the reductive N–O bond dissociation, potential energy curves are calculated as a function of the N–O separation, r_{N-O}, and the bond angle, ϕ_{N-N-O}, for both the N_2O and N_2O^- species. It has been shown that a simple model based on a two dimensional Morse curve description of the dissociative electron transfer appears adequate to assess the most essential features of this process [11,38]. From the superposition of the potential energy surfaces for neutral N_2O and the N_2O^- ion, obtained using the parameters reported by Hopper et al. [39], the transition state locus was determined by minimizing the activation energy, and taking into account constrains arising from the Frank-Condon principle. Electron transfer takes place at $r^*_{NO} = 1.28$ Å and $\phi_{N-N-O} = 153°$ for the gas phase reaction, while in the case of

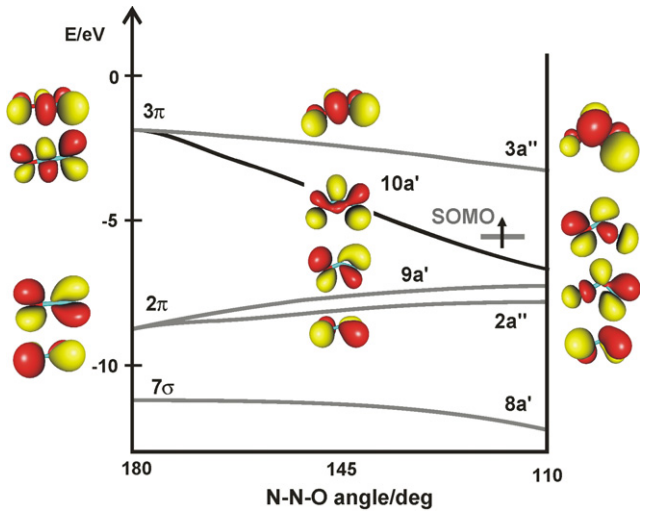

Fig. 1. Molecular orbital Walsh diagram of N_2O molecule with the SOMO level of tetra-coordinated molybdenum species constituting donor center. Please note the stabilization of the 10a′ ($3\pi^*$) orbital upon bending making the electron transfer energetically feasible.

surface ET at $r^*_{NO} = 1.23$ Å and $\phi_{N-N-O} = 160^\circ$ [11]. Owing to the shallow minimum in N_2O^- potential energy surface this species can appear as a temporal intermediate, which then spontaneously dissociates since the FC crossing point is situated above the N_2O^- dissociation limit. This means that the N–O bond breaking process does not occur simultaneously with ET and large activation energy of the N–O bond breaking is circumvented by vibronic pre-activation of the N_2O molecule (excitation of v_2 bending mode to reach the FC locus).

In conclusion, there are two principal coordinates for the observed reductive dissociation of nitrous oxide: the N–O bond elongation, which defines the dissociation pathway and the N–N–O bond bending that actually triggers the crucial electron transfer yielding, through a N_2O^- transient, the key O^- intermediate. Thus, to prompt the N_2O decomposition, the catalyst active site should exhibit there functionalities: high affinity toward N_2O binding, appropriate redox orbitals for efficient electron shuttling between the active centers, the reactants and intermediates (N_2O, O^-), and magnetic properties for spin catalysis. This latter point will be discussed in more detail in the next section.

3.1.2. Oxygen atom transfer route

Anionic oxygen transfer pathway of N_2O decomposition is essentially based on two processes: spin allowed N–O bond breaking

$$N_2O(^1\Sigma^+) + O^{2-}{}_{surf} \rightarrow N_2{}^{\uparrow}(^1\Sigma_g{}^+) + O_2{}^{2-}{}_{surf}(^1\Sigma_g{}^+)$$

and spin forbidden recombination of the resultant peroxide intermediates

$$O_2{}^{2-}{}_{surf}(^1\Sigma_g{}^+) + O_2{}^{2-}{}_{surf}(^1\Sigma_g{}^+) \rightarrow 2O^{2-}{}_{surf} + O_2{}^{\uparrow}(^3\Sigma_g{}^-)$$

The reactivity of the catalyst is related to the ability of surface oxygen anions to abstract the oxygen atom from N_2O molecule to form $O_2{}^{2-}$ species. Both steps the atom transfer and recombination of the peroxide ions were modeled by DFT on the (1 0 0) plane of MgO using the $Mg_{40}O_{40}(PC_{1836})$ cluster. Reaction modeling was corroborated by TPSR studies of N_2O decomposition on magnesium oxide. The molecular adsorption of N_2O takes place with no barrier but is rather weak, as it may be expected (the calculated binding energy was about 10 kcal/mol). The peroxide intermediate is produced via bent transition state NN–O–$O^{2-}{}_{surf}$ with the NN–O bond stretched from 1.18 to 1.48 Å, and at the O–$O^{2-}{}_{surf}$ distance of 1.75 Å. Further approach of the oxygen atom to the surface results in N–O bond splitting and the formation of the incipient $O_2{}^{2-}$ species with the O–O intermolecular bond length decreased to 1.45 Å. A more detailed insight into the intimate mechanism of the oxygen atom transfer can be inferred from the analysis of the evolution of the bond orders and the atomic partial charges along the reaction coordinate (Fig. 2). Inspection of Fig. 2a shows that while the ON–N bond remains practically intact during the reaction, the O–NN bond is produced at the expense of the O–O bond, as expected. Particular feature of this bond rearrangement is that it occurs in a narrow range of the O–O distances, indicating a hard nature of the involved interactions.

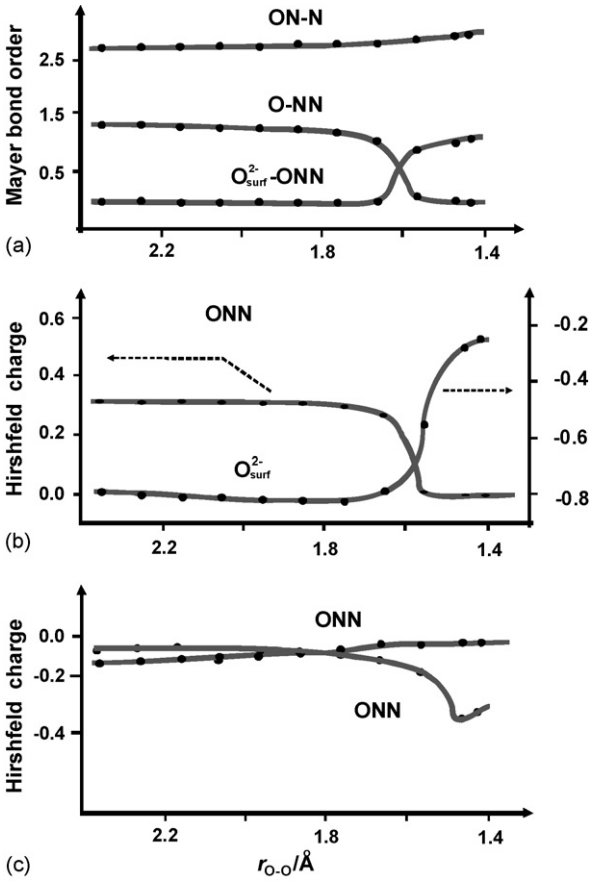

Fig. 2. Evolution of the bond orders of N–NO, NN–O, NNO–$O^{2-}{}_{surf}$ (a) and the atomic partial charges on middle nitrogen N**N**O and surface oxygen $O^{2-}{}_{surf}$ atoms (b) and terminal nitrogen **N**NO and oxygen NN**O** atoms (c) along the reaction coordinate of N_2O decomposition over MgO.

More striking changes were observed in the case of the charge redistribution (Fig. 2b and c). For the oxygen atom in the N_2O reactant, only small changes from $q_{ONN} = -0.04$ (in the intact molecule) to -0.25 (in the peroxide intermediate) were observed. The partial charge on the terminal nitrogen q_{ONN} is close to null and remains practically unchanged during the reaction course. However, the greatest changes take place on the middle nitrogen (from $q_{ONN} = 0.31$ to 0.0) and the surface oxygen (from $q^{2-}_O = -0.83$ to -0.27), showing that the main flow of the charge occurs between these two atoms. It may be then concluded that the N_2O dissociation via oxygen transfer mechanism is triggered by mutual compensation of the positive charge in the middle nitrogen atom and the negative charge on the surface O^{2-} ion.

The recombination pathway of two peroxo surface species producing an eventual O_2 molecule is shown in Fig. 3a. The reaction energetics is plotted as a function of the O–O distance (r_{O-O}) for the singlet and triplet state of the nascent dioxygen. Along the reaction coordinate two characteristic turning points can be distinguished at different r_{O-O} values. At larger distance ($r_{O-O} = 1.88$ Å) the curve crossing in singlet state creates the activation barrier for the recombination, whereas at shorter distance (close to that of O_2) there is an intersystem crossing from the spin singlet to the triplet one, characteristic of molecular

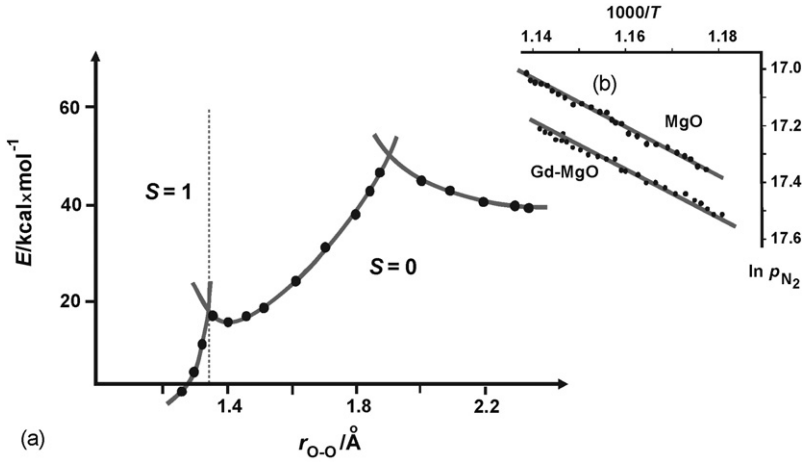

Fig. 3. Energetics of the surface recombination of peroxide ions as a function of O–O distance (r_{O-O}) for the singlet and triplet state of the nascent dioxygen (a). Arrhenius plot of N_2O decomposition over MgO and 1 wt.% Gd-doped MgO (b).

oxygen in its ground state ($^3\Sigma_g^-$). Since the energetic and the spin barriers are separated along the reaction coordinate, the recombination process can be accelerated by promoting the intersystem crossing using the concepts of spin catalysis [40]. This premise was checked in practice by impregnation of MgO surface with the Gd^{3+} ions [$4f^7$]. Owing to its seven unpaired electrons the trivalent gadolinium exhibits high magnetic moment generating inhomogeneous local magnetic fields, $B_{loc} \sim \mu/r^3$. The resultant uneven precession of both electronic spins (α, β) in the incipient oxygen molecule facilitates change in their mutual orientation from coplanar out of phase – characteristic of singlet state ($S = 0$, $M_S = 0$) to coplanar in phase – characteristic of triplet state ($S = 1$, $M_S = 0$). Therefore, such magnetic promotion should enhance the pre-exponential factor κ in the rate equation without changing the activation energy. The TPSR results (Fig. 3b) of N_2O decomposition over bare and 1 wt.% Gd-doped MgO in the conversion range 30–60%, presented in Arrhenius coordinates, provide a sound experimental support for this theoretical conjecture. Indeed, in the plot the slopes (corresponding to activation energies of $E_a = 16 \pm 1$ kcal mol^{-1}) of both lines are the same, whereas the pre-exponential factor is distinctly lowered upon Gd doping. As a result in the latter case the same conversions can be achieved at temperature lower by 130 K.

3.2. Molecular processes involving intrazeolite nitrosyl complexes and their mechanistic relevance for deNO$_x$ reaction

3.2.1. Nitroside and nitrosonium pathways of NO activation

The binding of nitric oxide to a transition metal center imparts unique catalytic chemistry both to the metal and the nitrosyl ligand itself [41]. To provide a more general picture of the uniqueness of metal-nitrosyl interfacial chemistry, a molecular level understanding of the bonding and reactivity of such species is necessary. At first we have to consider the molecular and electronic structures of transition metal nitrosyls encaged in the ZSM-5 zeolite and the interrelationship of nitrosyl bonding mode and the coordination geometry.

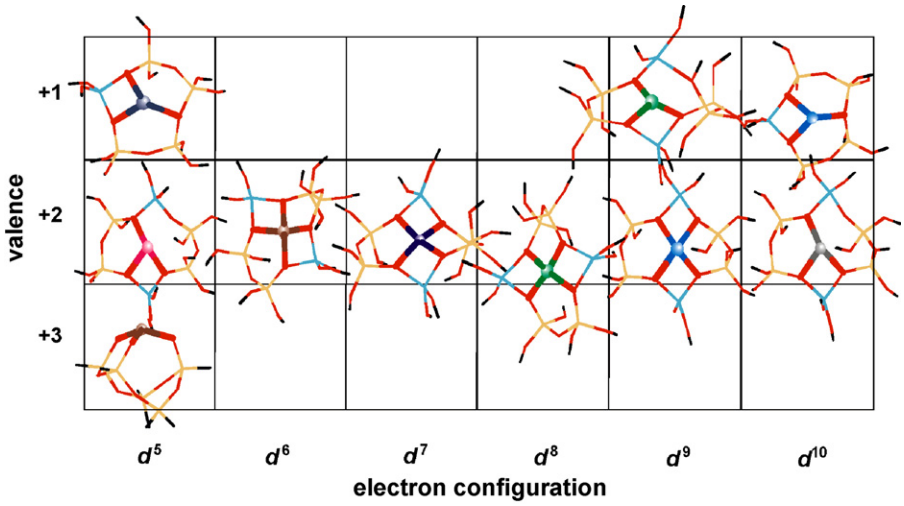

Fig. 4. Survey of the coordination environments of selected transition metal ions within the MFI framework as a function of their oxidation state and electronic configuration.

The following first series transition metals of different electron configuration and spin multiplicity hosted in ZSM-5 zeolite were chosen for the DFT investigations: Fe^{3+}, Mn^{2+}, Cr^{+} (d^5, ^6S), Fe^{2+} (d^6, ^5D), Co^{2+} (d^7, ^4F), Ni^{2+} (d^8, ^3F), Ni^{+}, Cu^{2+} (d^9, ^2D), and Cu^{+}, Zn^{2+} (d^{10}, ^1S). The results of our calculations revealed that both the electron and the spin states influenced the structure of the TMI sites. Generally the cations of semi-(d^5) and fully occupied valence shell (d^{10}) exhibit a three-fold coordination, whereas the $d^{6–9}$ metals are linked to the zeolite framework by making four bonds with framework oxygens (Fig. 4). The $^1Cu^+$/**M5** centers of planar trigonal coordination making two longer (2.025 and 2.047 Å) and one shorter (1.980 Å) bonds with the oxygen and tetra-coordinated $^4Co^{2+}$/**Z6** sites with four basal oxygen ligands ($<d_{Co–O}>$ = 2.06 Å), may serve here as an illustration. Going from low to high spin states, the coordination number decreases form C.N. = 4 to C.N. = 3. This was observed for, e.g., in Mn^{2+}/**Z6**, where $^6Mn^{2+}$ ion with sextet ground state assumes a nearly planar three-fold coordination, which turns into a tetragonal one for quartet and doublet states. The changes in the coordination are accompanied by decrease of the average metal–ligand distance from 2.162 Å to 2.026 and 1.996 Å, respectively. Analogous tetra- to tri-coordination switch is also observed on passing from $^4Cr^+$/**M5** to $^6Cr^+$/**M5** and $^3Ni^{2+}$/**Z6** to $^1Ni^{2+}$/**Z6**.

Interaction of nitric oxide with surface complexes of the investigated transition-metal ions leads to an isodesmic (i.e. preserving the coordination number) formation of the corresponding intrazeolite nitrosyl complexes at low pressures. This has been well documented experimentally, mainly by IR and EPR spectroscopies, as many of those species are paramagnetic [6,36,42]. Generally, the bonding of the M–NO moiety has been described by assigning formal oxidation states to the metal M and the nitrosyl ligand. In such assignment, the linear species posses a bound NO^+ (nitrosonium cation, a formal 3 electron donor), while a bent M–NO is deemed to posses a bound NO^- (nitroside anion, a formal 1 electron donor) [43]. However, such simple picture is often misleading and understanding the nature of the M–NO bond requires a more adequate quantum chemical approach. Because of the paramagnetic nature of NO (due to the doublet ground state $^2\Pi$) its coordination occurs not only through changes in the electron distribution but also involves associated changes in the spin density partition within the M–NO unit. We have identified the following prototype magnetic pathways of NO coordination:

(i) spin addition: $^1Cu^+$/**M5** + $^2NO \rightarrow \eta^1\{^2CuNO\}^{11}$/**M5**

S + D → D

(ii) spin pairing: $^5Fe^{2+}$/**Z6** + $^2NO \rightarrow \eta^1\{^4FeNO\}^7$/**Z6**

Qi + D → Q

(iii) spin pairing coupled with internal spin crossing:

$^4Co^{2+}$/**Z6** + $^2NO \rightarrow \eta^1\{^1CoNO\}^8$/**Z6**

Q + D → S

where S = singlet, D = doublet, Q = quartet, Qi = spin quintet. The resultant mononitrosyl complexes have been identified and characterized by EPR ($\eta^1\{CuNO\}^{11}$/ZSM-5 ($g_x = 1.999$, $g_y = 2.003$, $g_z = 1.889$, $A_x^{Cu} = 16\,mT$, $A_y^{Cu} = 15.5\,mT$, $A_z^{Cu} = 20.5\,mT$, $A_x^N = 3.0\,mT$, $A_y^N = 0.43\,mT$, $A_z^N = 0.55\,mT$), $\eta^1\{FeNO\}^7$/ZSM-5 ($g = 4$, $E/D < 1$ [44]) and IR spectroscopies $\eta^1\{CoNO\}^8$/ZSM-5 ($\upsilon_{exp} = 1857\,cm^{-1}$, $\upsilon_{calc} = 1863\,cm^{-1}$).

The structural characteristics of the investigated mononitrosyls indicate that they can be assigned into three generic classes of adducts: (i) ligand-centered radical complexes $\eta^1\{CuNO\}^{11}$; (ii) metal-centered radical complexes $\eta^1\{NiNO\}^9$, $\eta^1\{FeNO\}^7$, $\eta^1\{FeNO\}^6$; and (iii) diamagnetic $\eta^1\{CoNO\}^8$ complexes. In all cases the nitrosyl adducts exhibit bent geometries. The smallest value of the M–N–O angle ($\alpha = 123^\circ$) was observed for $\eta^1\{NiNO\}^9$ adduct while the largest one ($\alpha = 171^\circ$) for $\eta^1\{CrNO\}^6$. Thus, apparently the electronic configuration strongly influences the structure of the M–N–O moiety on passing from d^5 to d^{10}.

The binding of NO is exoergic by 29 kcal/mol for Fe^{3+} and Mn^{2+} with semi-occupied orbitals and increases to 35 kcal/mol for Co^{2+}, Ni^{2+}, Cu^+, and even to 50–53 kcal/mol for low valent Cr^+ and Fe^{2+} ions (Fig. 5). Nitric oxide coordinates to monovalent copper in an oxidative way ($\Delta Q_{Cu} = 0.08$), similarly to chromium and nickel(I). On the contrary, the rest of the transition metal ions are reduced ($\Delta Q_M = -0.22/-0.03$) upon the adsorption. The strongest reduction of the metal center is observed in the case of trivalent iron ($\Delta Q_M = -0.227$). Activation of the N–O bond of the nitrosyl ligand (gauged by changes in the N–O bond distance, bond order and its polarization, shown in Table 1) depends on the mode of its

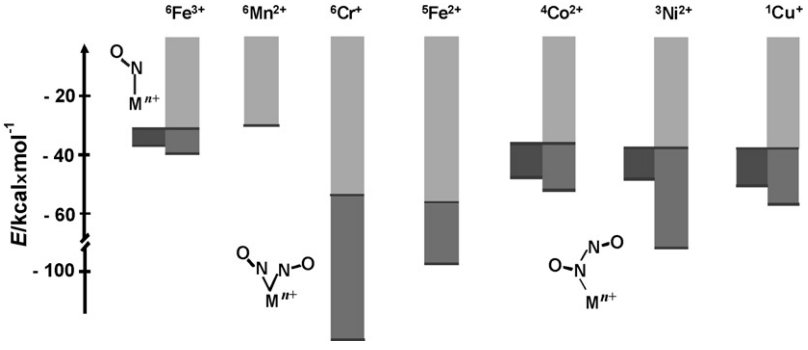

Fig. 5. The energy histogram for mononitrosyl (pale gray), dinitrosyl (gray) and dinitogen dioxide (dark grey) intrazeolite complexes with selected transition metal ions.

Table 1
Molecular parameters for mono- and dinitrosyl complexes of selected transition metal ions encaged within ZSM-5 zeolite

Adduct	d_{NO} (Å)	ΔQ_M	ΔQ_{NO}	ρ_M	ρ_{NO}	α_{MNO}	b_{N-O}	P_{NO}
$\{^3CrNO\}^6$	1.208	+0.099	−0.280	2.470	−0.514	171	1.725	0.021
$\{^3MnNO\}^6$	1.171	−0.143	+0.045	2.449	−0.509	167	1.947	0.042
$\{^3FeNO\}^6$	1.173	−0.227	+0.073	1.894	−0.325	153	1.913	0.056
$\{^4FeNO\}^7$	1.161	−0.126	+0.118	3.209	−0.576	168	2.031	0.034
$\{^1CoNO\}^8$	1.164	−0.141	+0.138	0	0	141	1.915	0.059
$\{^2NiNO\}^9$	1.155	−0.049	+0.134	0.775	−0.110	123	2.141	0.053
$\{^1NiNO\}^{10}$	1.166	+0.073	+0.065	0	0	165	1.950	0.068
$\{^1CuNO\}^{10}$	1.145	−0.031	+0.249	0	0	130	2.200	0.008
$\{^2CuNO\}^{11}$	1.181	+0.082	−0.020	0.120	0.932	151	2.097	0.020
$\{^2ZnNO\}^{11}$	1.162	−0.083	0.171	0.056	0.919	122	2.374	0.028
$\{^2Cr(NO)_2\}^7$	1.188	0.09	−0.13	1.41	−0.22	176		
	1.185		−0.11		−0.23	171		
$\{^2Fe(NO)_2\}^7$	1.155	−0.31	0.18	0.97	−0.05	170		
	1.166		0.14		−0.25	123		
$\{^1Fe(NO)_2\}^8$	1.174	−0.13	0.04	0	0	145		
	1.161		0.14			173		
$\{^2Co(NO)_2\}^9$	1.155	−0.12	0.18	1.08	−0.18	149		
	1.166		0.14		0.08	134		
$\{^1Ni(NO)_2\}^{10}$	1.164	−0.06	0.17	0	0	123		
	1.159		0.19			125		
$\{^1Cu(NO)_2\}^{12}$	1.184	0.08	−0.03	0	0	136		
	1.171		0.04			126		

d_{NO}, bond distance; ΔQ_M, ΔQ_{NO}, change in partial charge on metal and NO ligand; ρ_M, ρ_{NO}, spin density on metal and NO ligand; α_{MNO}, M–N–O bending angle; b_{N-O}, NO bond order; P_{NO}, polarization of NO bond.

coordination. The oxidative adsorption gives rise to the formation of a bound $NO^{\delta-}$ species (*nitroside pathway of activation*), while the reductive one to $NO^{\delta+}$ species (*nitrosonium pathway of activation*). In the latter case the highest changes in the activation parameters were observed for the $\eta^1\{NiNO\}^9$ and $\eta^1\{CoNO\}^8$ adducts. In both cases the M–N–O moiety is highly bent (130–140°), the N–O bond length shortened and its polarization increased by about three times in comparison to the free NO molecule. Such changes indicate that the NO acquires electrophilic properties upon the coordination. In contrast for $NO^{\delta-}$ species, the N–O bond is elongated, the N–O stretching frequency decreased, and the NO bond is only slightly polarized. Such changes indicate that the activation consists in redistribution of the electron density within the σ, π and 3d system, which accumulates on the nitrogen atom. The mechanistic implications of such situation are discussed in the next section.

3.2.2. Formation of the N–N bond

As discussed above the reactivity of the nitrosyl adducts is strongly related to the NO coordination mode and the electron and spin configurations of the metal center. Since formation of the N–N bond requires at least the vicinity of two NO ligands, we have explored two possible pathways along which the second NO molecule can be attached to the mononitrosyl complexes. They involve an attack on the metal (*inner-sphere addition*) giving rise to dinitrosyl adducts or an attack on the NO ligand (*outer-sphere coupling*) leading directly, through a bound N_2O_2 intermediate, to the N–N bond formation. Thus, the problem of developing a reactive charge distribution on a coordinated NO molecule essentially depends on the type of attack [45].

From the DFT calculations of the investigated transition metal mononitrosyls it can be inferred that the spin density distribution within the M–NO moiety is a primary factor directing the NO attack on the metal or on the NO ligand. For those nitrosyls, which exhibit the spin localized mainly on the metal (Cr^+, Fe^{2+} and Fe^{3+}, Ni^{2+}), there is a preference toward the formation of the dinitrosyl species, whereas for the $\eta^1\{CuNO\}^{11}$ and $\eta^1\{ZnNO\}^{11}$ adducts, which belong to ligand-centered radicals, an outer-sphere coupling is favored.

The energetics of the inner- and outer-sphere routes of the second NO molecule binding is shown in Fig. 5. For the Fe^{2+} and Cr^+ centers the dinitrogen dioxide adducts were found to be unstable, whereas in the case of Co^{2+}, Ni^{2+} and Cu^+ centers their formation is favorable by about 10 kcal/mol. Although this indicates that such sites are capable for knitting the N–N link, they clearly exhibit stronger thermodynamic preference toward the formation of dinitrosyls, wherein the coordination does not lead to a direct N–N bond making.

To further explore the mechanistic relevance of both types of complexes we have analyzed the structure–reactivity relationships for dinitrosyl species in more detail. Formation of dinitrosyl adducts is oxidative for Fe, Co and Ni ($\Delta Q_M = -0.29/-0.06$), whereas in the case of copper it is reductive ($\Delta Q_{Cu} = 0.08$), similarly to the corresponding mononitrosyls. The highest

bending of the M–N–O angle (α = 123–124°) was observed for $\eta^1\{Ni(NO)_2\}^{10}$ with both NO ligands coordinated formally as nitrosonium cations ($\upsilon_s^{exp} = 1882\,cm^{-1}$, $\upsilon_{as}^{exp} = 1841\,cm^{-1}$ and to $\upsilon_s^{theo} = 1856\,cm^{-1}$, $\upsilon_{as}^{theo} = 1807\,cm^{-1}$ bands). None of the investigated complexes possessed a distinct *cis*-coplanar structure with one linear and one bent NO moiety, which is required by the MO symmetry restrictions for the concerted decomposition of two NO molecules to N_2 and O_2 [41,43,45].

Conformation analysis of the dinitrosyls gives another important indication concerning their potential mechanistic relevance for *de*NO_x activity. The dinitrosyl complexes can exhibit two bent conformations referred to as *attracto* and *repulso* [41]. In the *attracto* geometry the oxygen atoms are angled to each other, whereas both nitrogens are drawn aside. The situation is reversed in the *repulso* conformation. Both oxygen atoms are far-off and the nitrogen atoms are close to each other. Energetically for the monovalent copper the *attracto* conformation is favored over the *repulso* by 7.7 kcal/mol. These two forms can be easily distinguished in IR spectroscopy by the diagnostic intensity ratio of symmetric (1732 cm^{-1}) and antisymmetric (1826 cm^{-1}) stretching bands. The DFT calculations have shown that for the *attracto* conformation both intensities are comparable, whereas for the *repulso* conformer the intensity of symmetric stretching dominates the spectrum. Since in the experimental IR spectra the intensities of the both bands are similar, this is indicative for presence of the *attracto* complex, in accordance with the theoretical predictions. However, more detailed analysis reveals that this form appears to be chemically inert. Indeed, the DFT modeling showed that despite the proximity of both oxygen atoms, further decreasing of the O–O distance for potential bond forming is accompanied by simultaneous accumulation of the positive charge on both atoms. As the result the energy of the system drastically increases. The accumulation of the positive charge on the terminal oxygens prevents the formation of O–O bond, and apparently the orbital symmetry barrier is replaced here by Coulombic repulsion barrier.

Alternative formation of the N–N bond (instead of O–O) requires an isomerization from the *attracto* to *repulso* conformation, which is an activated process with the barrier of 13 kcal/mol. Subsequent transformation of the *repulso* complex to $\eta^2\{CuN_2O_2\}^{12}$, tantamount with the nascence of the N–N bond, requires rather small activation energy (6.6 kcal/mol). Since direct creation of the N–N bond via outer-sphere attack (via N_2O_2 transient) is non-activated, we may then conclude that the thermodynamically more stable dinitrosyls are mere spectators, whereas the dinitrogen dioxide transient appears to be the actual reactive species. The IR spectra provide a requisite experimental support for this theoretical analysis. While in the static conditions both mono- and dinitrosyls are readily observed at 100 K, in the operando regime at 573 K only copper mononitrosyl and nitrates, but not dinitrosyls, have been detected [46]. The nitrates are terminal intermediates involved in the O–O bond formation step of the *de*NO_x cycle and thus apparently produced without involvement of dinitrosyl intermediates [5,46].

4. Conclusions

Combination of molecular modeling with computational spectroscopy provides a powerful bottom-up approach to the chemistry of making and breaking of N–O, N–N and O–O bonds. Two basic mechanisms of N_2O dissociation based on electron and oxygen atom transfer can be distinguished. The N–N–O bond bending is imperative not only for triggering the electron transfer, yielding through N_2O^- transient the key O^- intermediate, but also for the energetic feasibility of this process. In the oxygen atom transfer route of N_2O decomposition, recombination of the surface peroxide intermediate can be accelerated using the spin catalysis. The activation of NO occurs in an oxidative (*nitrosonium complexes*) or reductive (*nitroside complexes*) way depending on the electronic configuration and the spin state of the transition metal ions. The spin density repartition within the M–N–O moiety appears to be a primary factor determining the direction of the addition of second NO molecule and its binding. The N–N bond may be formed via an inner-sphere process with the formation of $\eta^2\{M(NO)_2\}^n$ or through an outer-sphere coupling leading to $\eta^1\{MN_2O_2\}^n$ intermediates. In the case of Cu-ZSM-5 the latter mechanism is kinetically favored.

Acknowledgements

This work was supported by the Committee for Scientific Research of Poland, KBN, project number 3 T09A 147 26. The calculations were performed with the computer facilities of CYFRONET–AGH, grant number KBN/SGI2800/UJ/018/2002. P. Pietrzyk thanks the Prime Minister of Poland for Ph.D. Thesis Award.

References

[1] M. Iwamoto, H. Hamada, Catal. Today 10 (1991) 57.
[2] F. Kaptein, J. Rodriguez-Mirasol, J.A. Moulijn, Appl. Catal. B 9 (1996) 25.
[3] C.S. Swamy, J. Christofer, Catal. Rev. -Sci. Eng. 34 (1992) 409.
[4] B. Moden, P. Da Costa, D. Ki Lee, E. Iglesia, J. Phys. Chem. B 106 (2002) 9633.
[5] B. Moden, P. Da Costa, B. Fonfe, D. Ki Lee, E. Iglesia, J. Catal. 209 (2002) 75.
[6] J.H. Lunsford, The Catalytic Chemistry of Nitrogen Oxides, Plenum, New York, 1975.
[7] C. Prestipino, G. Berlier, F.X. Llabres i Xymena, G. Spoto, S. Bordiga, A. Zscchina, G. Turnes Palomino, T. Yamamoto, C. Lamberti, Chem. Phys. Lett. 363 (2002) 389.
[8] A. Heyden, B. Peters, A.T. Bell, F.J. Keil, J. Phys. Chem. B 106 (2005) 1857.
[9] Y. Li, J.N. Amor, Appl. Catal. B 3 (1993) 55.
[10] R.G. Pearson, Acc. Chem. Res. 4 (1971) 152.
[11] Z. Sojka, M. Che, J. Phys. Chem. 100 (1996) 14776.
[12] E.J. Karlsen, M.A. Nygren, L.G.M. Pettersson, J. Phys. Chem. A 106 (2002) 7868.
[13] A. Ribera, I. Arends, S. de Vries, J. Perez-Ramirez, R.A. Sheldon, 195 (2000) 287.
[14] G.I. Panov, V.I. Sobolev, K.A. Dubkov, A.S. Kharitonov, Stud. Surf. Sci. Catal. 101 (1996) 493.
[15] A. Satsuma, R. Akahori, M. Kato, S. Komai, H. Yoshida, T. Hattori, J. Mol. Catal. A 155 (2000) 81.
[16] CASTEP Users Guide, Accelrys Inc., San Diego, 2001.

[17] V. Milman, B. Winkler, J.A. White, C.J. Pickard, M.C. Payne, E.V. Akhmatskaya, R.H. Nobes, Int. J. Quant. Chem. 77 (2000) 895.
[18] H.B. Schlegel, in: K.P. Lawley (Ed.), Ab initio Methods in Quantum Chemistry—I, Wiley, New York, 1987.
[19] F.L. Hirshfeld, Theor. Chim. Acta B 44 (1977) 129.
[20] E.R. Davidson, S. Chakravorty, Theor. Chim. Acta 83 (1992) 319.
[21] DMol^3, Quantum-chemical software, Molecular Simulations, Inc., 1999.
[22] B. Delley, J. Chem. Phys. 92 (1990) 508.
[23] S.H. Vosko, L. Wilk, M. Nusair, Can. J. Phys. 59 (1990) 1200.
[24] I. Mayer, Chem. Phys. Lett. 97 (1983) 270.
[25] A. Snis, H. Miettinen, J. Phys. Chem. B 102 (1998) 2555.
[26] A.D. Becke, Phys. Rev. A 38 (1988) 3098.
[27] J.P. Perdew, in: P. Ziesch, H. Eschrig (Eds.), Electronic Structure of Solids '91, Akademie Verlag, Berlin, 1991.
[28] G. te Velde, F.M. Bickelhaupt, S.J.A. van Gisbergen, C. Fonseca Guerra, E.J. Baerends, J.G. Snijders, T. Ziegler, J. Comput. Chem. 22 (2001) 931.
[29] C. Fonseca Guerra, J.G. Snijders, G. te Velde, E.J. Baerends, Theor. Chem. Acc. 99 (1998) 391.
[30] ADF2004.01, SCM, Theoretical Chemistry, Vrije Universiteit, Amsterdam, The Netherlands (http://www.scm.com).
[31] E. van Lenthe, E.J. Baerends, J.G. Snijders, J. Chem. Phys. 99 (1993) 4597.
[32] C. van Wüllen, J. Comput. Chem. 23 (2002) 779.
[33] M.J. Frish, et al., Gaussian03, revision B.05, Gaussian, Inc., Pittsburgh, PA, 2003.
[34] T. Spalek, P. Pietrzyk, Z. Sojka, J. Chem. Inf. Model. 45 (2005) 18.
[35] Z. Sojka, M. Che, J. Phys. Chem. 99 (1995) 5418.
[36] Z. Sojka, M. Che, E. Giamello, J. Phys. Chem. B 101 (1997) 4831.
[37] M. Che, Z. Sojka, Top. Catal. 15 (2001) 211.
[38] Z. Sojka, Appl. Magn. Reson. 18 (2000) 71.
[39] D.G. Hopper, A.C. Wahl, R.L.C. Wu, T.O. Tierman, J. Chem. Phys. 65 (1976) 5474.
[40] A.L. Buchachenko, V.L. Berdinsky, Chem. Rev. 102 (2002) 603.
[41] G.B. Richter-Addo, P. Legzdins, Metal Nitrosyls, Oxford University Press, New York-Oxford, 1992.
[42] K. Hadjiivanov, Catal. Rev. -Sci. Eng. 42 (2000) 71.
[43] R. Eisenberg, C.D. Mayer, Acc. Chem. Res. 8 (1975) 26.
[44] A.M. Volodin, K.A. Dubkov, A. Lund, Chem. Phys. Lett. 333 (2001) 41.
[45] R. Eisenberg, D.E. Hendriksen, Adv. Catal. 28 (1979) 79.
[46] M.V. Konturu, S.S.C. Chuang, J. Catal. 196 (2000) 271.